Drop-casted Platinum Nanocube Catalysts for Hydrogen Evolution Reaction with Ultrahigh Mass Activity

Bonhyeong Koo[+],[a] Jinwoo Chu[+],[a] Jongsu Seo,[a] Gihun Jung,[a] Seung Hee Baek,[b] Sung-Wook Nam,[b] Calem Duah,[c] Young Kuk Lee,*[c] WooChul Jung,*[a] and Byungha Shin*[a]

Platinum hydrogen evolution reaction (HER) electrocatalysts in the form of nanocubes (NCs) were synthesized at 50 °C by aqueous-based colloidal synthesis and were applied to electrochemical (EC) and photoelectrochemical (PEC) systems by a fast and simple drop-casting method. A remarkable Pt mass activity of 1.77 A mg^{-1} at −100 mV was achieved in EC systems (fluorine-doped tin oxide/Pt NC cathode) with neutral electrolyte while maintaining low overpotential and Tafel slope. In the Cu(In,Ga)(S,Se)$_2$ (CIGS)-based PEC system, a carefully chosen amount of Pt NC loading to achieve a compromise between the catalytic activity (more Pt NCs) and better light transmittance (fewer Pt NCs) led to a maximum onset potential of 0.678 V against the reference hydrogen electrode. The photoelectrodes with Pt NCs also exhibited good long-term operational stability over 9.5 h with negligible degradation of the photocurrent. This study presents an effective strategy to greatly reduce the use of expensive Pt without compromising the catalytic performance because the drop-casting of Pt NC solutions to form electrocatalysts is expected to waste less raw material than vacuum deposition.

Introduction

Photoelectrochemical (PEC) water splitting is expected to be an ideal method to produce hydrogen once the efficiency of the PEC system is improved and the production cost is greatly reduced.[1] An electrocatalyst is a critical component of a PEC system and it is often bound on the surface of a light-absorbing photoelectrode.[2] In the typical monolithic photoelectrode configuration, electrocatalysts are placed on the side where light is incident.[3–5] Therefore, not only catalytic activity but also light transmittance is an important factor to consider when designing an electrocatalyst-coated photoelectrode system.

For the hydrogen evolution reaction (HER) and oxygen reduction reaction (ORR), Pt is the best choice as far as the catalytic performance is concerned. A variety of non-precious materials, such as metals (Fe,[6] Co,[7,8] Ni[9]), oxides (NiO$_x$,[10] Cu$_x$O[11,12]), sulfides,[13] carbides,[14] nitrides,[15] phosphides,[16] carbonaceous materials,[17] oxysulfides,[18] and oxynitrides,[19] have been studied to replace Pt. However, none has so far surpassed the catalytic activity of Pt. An obvious alternative approach is reducing the use of Pt, that is, improving the mass activity of Pt by forming a nanostructure with a high surface-to-volume ratio, such as nanoparticles,[5] nanowires,[20] patterned islands,[21] an atomic monolayer,[22] or even a collection of single atoms.[23–25] However, the past studies on forming nanostructured Pt encountered some issues such as inferior performance[26] and complex and/or harsh processing conditions[22] for the catalyst synthesis. Considering the chemical or thermal vulnerability of many photoelectrode materials, it would be advantageous if the application of electrocatalysts could be carried out in mild conditions.

Here, we report on the use of Pt nanocubes (NCs) as electrocatalysts for HER, which allowed us to achieve a mass activity of 1.77 A mg^{-1} of Pt at an applied voltage of 0.10 V vs. reversible hydrogen electrode (RHE) while maintaining an overpotential and a Tafel slope comparable to reported state-of-the-art Pt-based catalysts. Pt NCs were synthesized by aqueous-based colloidal synthesis at 50 °C and dispersed onto a (photo)electrode by a drop-casting method, which is cost-effective, fast, and free of damage to the underlying material. Furthermore, drop-casting wastes less raw material compared to vacuum deposition techniques. Pt NCs were also applied to Cu(In,Ga)(S,Se)$_2$ (CIGS) photocathode-based PEC HER. A compromise between the light transmittance (less loading of Pt NCs) and the catalytic activity (more Pt NCs) led to an impressive onset potential of 0.678 V_{RHE} from Pt NC-coated CIGS-based photocathode.

Results and Discussion

Pt nanocubes (Pt NCs) were synthesized by aqueous-based colloidal synthesis using a solution consisting of a Pt-containing precursor (K_2PtCl_4), cationic surfactants (alkyltrimethylammonium bromide, C_nTABr), and reducing reagents

[a] Dr. B. Koo,[+] J. Chu,[+] J. Seo, G. Jung, Prof. W. Jung, Prof. B. Shin
Department of Materials Science and Engineering
Korea Advanced Institute of Science and Technology (KAIST)
Daejeon 34141 (Republic of Korea)
E-mail: wcjung@kaist.ac.kr
byungha@kaist.ac.kr
[b] S. H. Baek, Prof. S.-W. Nam
School of Medicine
Kyungpook National University
Daegu 41405 (Republic of Korea)
[c] C. Duah, Dr. Y. K. Lee
Korea Research Institute of Chemical Technology
Daejeon 34114 (Republic of Korea)
E-mail: leeyoung@krict.re.kr
[+] These authors contributed equally to this work.

Supporting information for this article is available on the WWW under https://doi.org/10.1002/cssc.202100613

© 2021 Wiley-VCH GmbH

($NaBH_4$).[27,28] We prepared three different sizes of Pt NCs by varying chain lengths of the cationic surfactants and concentrations of the surfactants (Table S1), which we refer to as Pt NC_S ($D \approx 8$ nm), Pt NC_M ($D \approx 20$ nm), and Pt NC_L ($D \approx 25$ nm), where D denotes the average size of the NCs.

Figure 1a,b presents TEM and high-resolution TEM images of Pt NCs of different sizes. For Pt NC_M and Pt NC_L, it is evident that the predominant shapes of the NCs are cubes, bounded by {100} facets with some corners cut exposing {110} facets, and cuboctahedrons, bounded by {100} and {111} facets. Such facets did not fully develop in the case of Pt NC_S. Cyclic voltammetry (CV) measurements from the varying sizes of Pt NCs in an electrolyte of 0.5 M potassium phosphate buffer (KPi) are shown in Figure 1c. It has been known that peaks at 0.30 and 0.17 V in CV curves originate from hydrogen absorption or desorption on the {100} and {110} facets of Pt NCs in phosphate buffer, respectively.[29,30] Consistent with the TEM results, the CV results confirmed the formation of {100} and {110} facets for Pt NC_M and Pt NC_L while such a feature is absent for Pt NC_S.

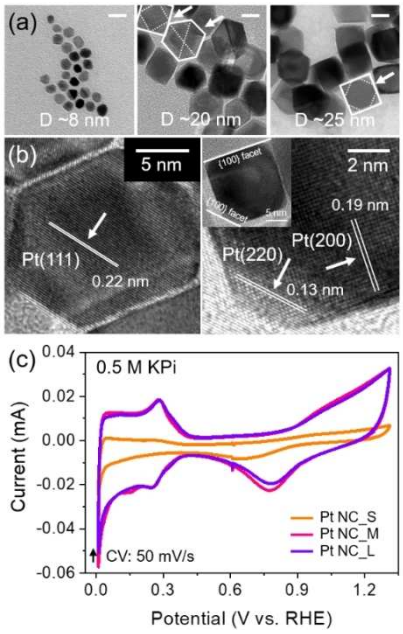

Figure 1. (a) TEM images of synthesized Pt nanocubes with various sizes. Scale bar is 10 nm. Cuboctahedron-shaped nanoparticles are indicated by an arrow. The dotted lines are to illustrate the images of a cuboctahedron when viewed along [100] or [110] directions (see Figure S1). (b) High-resolution TEM images of large-sized Pt nanocubes [a cuboctahedron in the left and a cube with a corner cut forming (110) plane]. (c) CV curves of Pt nanocubes of various sizes. Measurements were carried out in 0.5 M KPi as electrolyte.

Synthesized Pt NCs were coated on a fluorine-doped tin oxide (FTO)/glass substrate via drop-casting. A detailed description for forming the Pt electrocatalyst based on NCs is shown in the Experimental Section and Figure S2. In short, the drop-casting of a small quantity (5–20 μL) of the NC solution over a substrate of 0.5×0.8 cm^2 was repeated until a desired amount of Pt was loaded. We found that, compared to a single drop of a large quantity, repeated drop-casting of a smaller quantity resulted in more stable binding of Pt NCs onto the substrate. After the final drop-casting, a white stain was visible from the surface, which we were able to remove by rinsing with ethanol (Figure S3). Inductively coupled plasma mass spectrophotometry (ICP-MS) analysis before and after the ethanol rinsing showed that the rinsing selectively removed the stains with a minimal loss of Pt (≈6%) (Table S2).

Figure 2a–c presents linear sweep voltammetry (LSV) measurements of the prepared Pt cathodes with different repetition numbers of drop-casting of the NC solution (i.e., different loading of Pt catalysts) before and after the ethanol rinsing. A 0.5 M KPi solution was used as the electrolyte and a Pt coil as the counter electrode. In each case, the HER performance of the Pt electrode improved during the first several (typically three) LSV measurements, after which the LSV curve remained

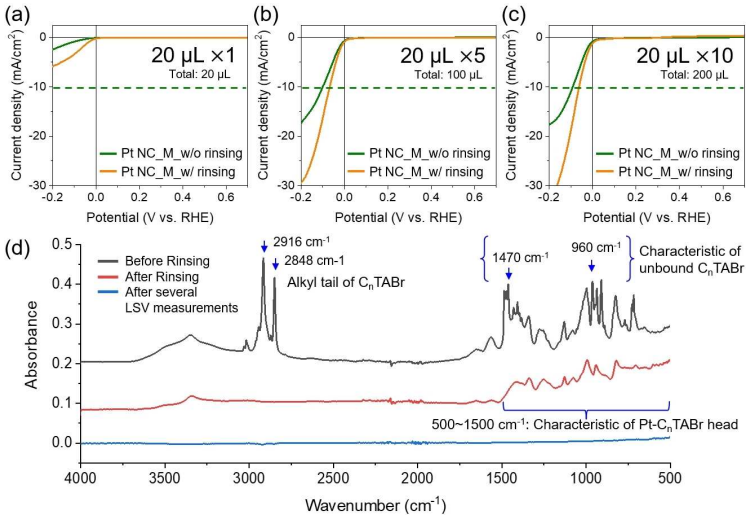

Figure 2. LSV measurements of Pt NC_M in 0.5 M KPi buffer solution before and after ethanol rinsing. In order to increase the loading of Pt NCs, NC solution was dropped repeatedly for: (a) 1 time (total 20 μL), (b) 5 times (total 100 μL), and (c) 10 times (total 200 μL). (d) FTIR spectra of Pt NC_M 100 μL before ethanol rinsing, after ethanol rinsing, and after several LSV measurements when the LSV curve started to remain unchanged.

© 2021 Wiley-VCH GmbH

unchanged (see Figure S4). The LSV curves of the Pt NCs presented in Figure 2a–c were acquired after reaching performance saturation with repeated LSV scans. Two observations are immediately noteworthy. First, there was significant improvement in the HER performance after the ethanol rinsing (i.e., with removal of the stain). Second, more loading of Pt, as anticipated, led to better HER activity; the improvement is less dramatic when the dropping volume increased from 100 to 200 μL compared to the change seen from 20 to 100 μL (Figure 2c).

To identify the chemical origin of the white stain observed from the as-prepared samples and the reason for the performance improvement with its removal, we performed X-ray photoelectron spectroscopy (XPS) and Fourier-transform infrared spectroscopy (FTIR) analyses before and after the ethanol rinsing. C 1s XPS spectra (Figure S5) showed substantial removal of carbon-based species after the ethanol rinsing. Additionally, the presence of potassium was observed in the sample before the rinsing. The most reasonable interpretation of these results is that the white stain consisted of residual C_nTABr ligands and residual potassium compounds present in the Pt precursor. Further confirmation of our identification of the white stain came from FTIR measurements. Based on a previous study, we identified that FTIR bands at 2916 and 2848 cm^{-1} were due to alkyl tails in tetradecyltrimethylammonium bromide (C_{14}TAB) and bands at 1450 and 760 cm^{-1} were from unbound C_{14}TAB molecules while broad bands between 500–1500 cm^{-1} were from C_{14}TAB heads bound to Pt NCs.[31] The FTIR spectrum after the ethanol rinsing revealed the removal of unbound C_nTABr molecules and alkyl tails of C_nTABr bound to Pt NCs (Figure 2d); however, C_nTABr heads still remained on the Pt NCs. After several LSV scans the broad FTIR bands related to the C_nTABr heads stuck on the NCs completely disappeared. In addition to the disappearance of C_nTABr, no other residual organic species were observed after the ethanol rinsing. The removal of C_nTABr ligands from the Pt electrode via the chemical (by ethanol) and electrochemical (by LSV scans) cleaning must be responsible for the improved HER performance.

From the results shown in Figure 2, we learned that minimal loading of Pt NCs whose HER performance become saturated was coating a total of near 100 μL NC solution (5 iterations of coating of 20 μL). In further experiments we fixed the volume of NC solutions drop-casted at 40, 80, and 120 μL. Samples are denoted as "Pt NC X Y μL", where X is for the size (S, M, or L) and Y is the total volume of NC solution used. Figure 3a,b presents the LSV curves and Tafel slopes of Pt NC_M samples. Both the overpotential, defined as the potential at the operating current of -10 mA cm^{-2}, and Tafel slope decreased with increasing Pt loading from 40 to 80 μL; however, with a further increase of the solution amount to 120 μL, there was negligible change in the performance. The mass of Pt used in each sample was measured by ICP-MS, the results of which is summarized in Table S3. With the measured masses of Pt, the mass activity of the samples as a function of the applied potential is presented in Figure 3c. Notably high mass activity was demonstrated from Pt NC_M 80 μL: 1.77 A mg^{-1} at an overpotential of -50 mV and 0.54 A mg^{-1} at -100 mV (Figure 3d), which are the highest among Pt-based catalysts for HER carried out in a neutral electrolyte (Table S4). Although Pt NC_M 120 μL exhibited a slightly enhanced Tafel slope, its mass activity was poorer than the other samples.

The superior catalytic performance of our Pt NCs was further confirmed by comparing with commercial Pt/C electrodes (20 wt% Pt). Figure S6 and Table S5 showed that with similar amounts of Pt used, commercial Pt/C showed much lower catalytic activity (overpotential: 0.1–0.15 V at 10 mA cm^{-2}, and Tafel slope: 70–85 mV dec^{-1}) than the drop-casted Pt NCs.

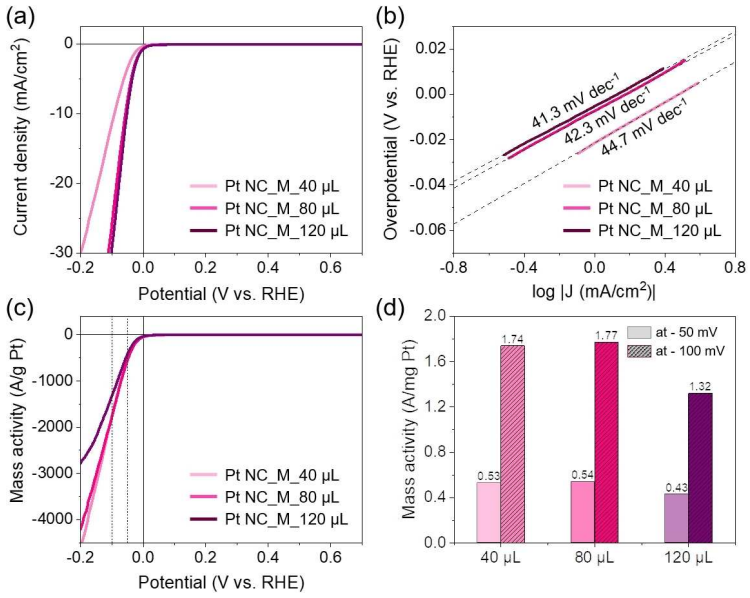

Figure 3. (a) LSV curves and (b) Tafel plots of Pt NC_M with three different dropping amounts in 0.5 M KPi buffer solution. (c) Mass activity vs. potential obtained by normalizing LSV curves by the mass of Pt used in each case. (d) Mass activity (A mg^{-1} Pt) at overpotential of -50 and -100 mV vs. RHE.

© 2021 Wiley-VCH GmbH

Next, we investigated the application of our Pt NCs as HER catalysts in a PEC system. We applied the Pt NCs onto a CIGS-based photocathode consisting of Mo/CIGS/ZnS/CdS/reduced graphene oxide(rGO). As the Pt NC solution is based on deionized (DI) water-based solution, it can be applied to various substrates, including CdS-coated CIGS, without causing any damage on the substrate. In our earlier studies, we applied a thin layer of ZnS between the CIGS and the CdS layers and greatly improved the PEC performance due to the alteration of surface band bending of the CIGS due to the diffusion of Zn into the CIGS.[32] We also introduced rGO, which can act as a catalyst binder when placed between CdS and Pt catalysts, greatly improving the operation stability of CIGS photocathodes.[33] Figure 4a presents LSV curves under illumination with different loading of medium-sized Pt NC by varying the total volume of NC solution that was drop-casted onto the CIGS photocathodes. With increasing Pt loading, the onset potential improved (i.e., increased toward the anodic direction), but the photocurrent density diminished due to the reduced light transmittance of the Pt layer (Figure S7). When a larger onset potential was desired (at some expense of the photocurrent), Pt NC_M 100 μL can be used instead of Pt NC_M 50 μL. We also examined the effects of the Pt NC size on the PEC performance while keeping the total loaded amount of NC solution the same. As shown in Figure 4b, there was slight variation in both the onset potential and photocurrent density; however, this variation appeared to be within the statistical fluctuation, as confirmed by the collection of PEC performance values of Pt NCs with various sizes and loading amounts (see Figure 4c for the summary and Figures S8 and S9 for the raw LSV curves). A similar trend of improved onset potentials and reduced photocurrent densities with larger volumes were observed regardless of the size of the Pt NCs. Finally, we evaluated the stability of CIGS/ZnS/CdS/rGO/Pt NCs by monitoring chopped chronoamperometry measurements. Pt NC_M 100 μL was used for the test and it lasted more than 9.5 h without any noticeable drop in the photocurrent density (Figure 4d).

Conclusions

With a simple and fast fabrication method consisting of drop-casting of Pt nanocubes (NC) solutions prepared by aqueous-based colloidal synthesis, we demonstrated both electrochemical (fluorine-doped tin oxide/Pt NCs cathode) and photoelectrochemical (PEC) [$Cu(In,Ga)(S,Se)_2$/ZnS/CdS/rGO/Pt NCs photocathode] hydrogen evolution reaction (HER) systems with remarkable catalytic performance (low overpotentials and Tafel slopes) and high stability (≈9.5 h) in a neutral electrolyte. Notably, very high mass activity of Pt for HER (1.77 A mg^{-1} at an overpotential of 100 mV and 0.54 A mg^{-1} at 50 mV) is demonstrated, which is the record value among Pt-based HER catalysts reported in the literature. In addition to the high catalytic performance, the proposed fabrication method can minimize the loss of the precious raw material, Pt. In the synthesis step of Pt NCs, there was a negligible loss of Pt because nearly all Pt particles were collected from the precursor solution during the centrifugation. In the drop-casting step, none of the Pt nanocube solution was wasted because all the solution was spread

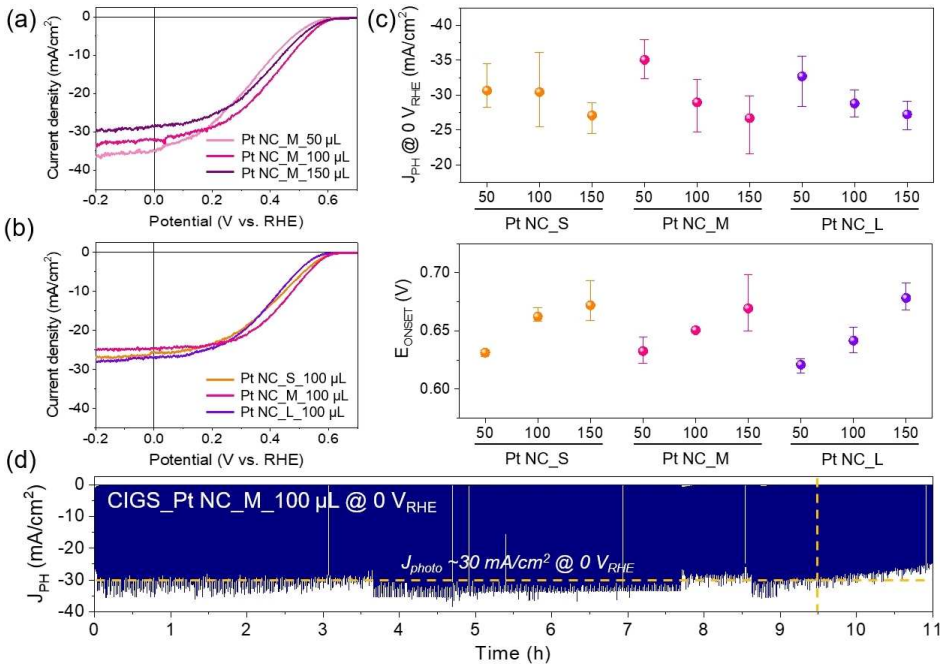

Figure 4. LSV curves, under 1 sun illumination, of CIGS/ZnS/CdS/rGO/Pt NC photocathode with (a) different dropping amount of medium-sized Pt NC, (b) different sizes of Pt NCs prepared by 100 μL NC solution. (c) Comparison of current density at 0 V vs. RHE and onset potential for different NC sizes and the dropping amount of NC solution. (d) Chopped chronoamperometry measurement of CIGS/ZnS/CdS/rGO/Pt NC_M 100 μL × 2 under 1 sun illumination at 0 V vs. RHE. Light chopping was done for every 30 s.

© 2021 Wiley-VCH GmbH

onto the whole area of a substrate. Finally, during the ethanol rinsing, about 6% loss of Pt was confirmed by inductively coupled plasma mass spectrophotometry, resulting in an average yield of the catalysts of approximately 94%. The presented method is also expected to be easily expandable to a large-scale, high-throughput process, thus paving a pathway towards the commercialization of hydrogen fuel production by PEC water splitting.

Experimental Section

Synthesis of C_{12}TABr template Pt nanocubes

Pt nanocubes stabilized with cationic surfactant (C_{12}TABr) were prepared through colloidal synthesis.[27,28] A solution mixture of C_{12}TABr (145 mM, 37.5 mL) and K_2PtCl_4 (9.1 mM, 5 mL) was put into a 100 mL round-bottomed flask and heated to 50 °C in an oil bath with continuous stirring at 300 rpm until the mixture became transparent. Then the flask was sealed with rubber septum, and ice-cooled aqueous solution of sodium borohydride ($NaBH_4$, 500 mM, 3 mL) as a reducing agent was added with a syringe. Through a needle of the syringe, H_2 gas generated in the flask was released for 20 min. The aqueous solution was kept at 50 °C during the reaction for 24 h. To refine Pt nanocubes from the solutions, the resulting brown solution was centrifuged at 12000 rpm for 15 min twice. The precipitates, Pt nanocubes, were collected and re-dispersed in 45 mL of deionized water.

Drop-casting of Pt nanocube solution

Pt nanocube solution was drop-casted onto a 5 mm ×8 mm substrate placed on a hot plate kept at 110 °C. A desired amount of the solution was drop-casted by multiple drops of 5–20 μL with natural drying after each dropping. After the repeated coating, the substrate was rinsed with ethanol until most of the covered white layer (C_nTABr) was removed. A schematic illustration of the procedure is provided in Figure S2.

Preparation of CIGS/ZnS/CdS/rGO photocathode

CIGS/ZnS/CdS/rGO was prepared as a photocathode for PEC HER. CIGS thin film was deposited on Mo-coated soda lime glass by co-sputtering of elemental sources, Cu, In, and Ga followed by selenization and sulfurization. ZnS and CdS buffer layers were then introduced by home-made chemical bath deposition. Reduced graphene oxide was spray-coated on the sample on a hot plate kept at 100 °C. A full description of the photocathode fabrication in more detail is available in our previous publication.[32]

Characterization

Shapes and sizes of synthesized Pt nanocubes were characterized with transmission electron microscopy (TEM, JEOL JEM-3010) and field-emission transmission electron microscopy (FE-TEM, FEI Company Titan G2 ChemiSTEM Cs Probe). XPS (Thermo VG Scientific Sigma Probe) and FTIR spectroscopy (Thermo Scientific Nicolet iS50) were employed to identify the surfactant content on an FTO substrate after the drop-casting of Pt nanocube solution, after ethanol rinsing, and after several electrochemical measurements. ICP-MS (Thermo Scientific iCAP RQ) measurement was carried to determine the total mass of Pt deposited on an FTO substrate for the calculation of mass activity. Light transmittance of various size and amount of Pt NC loaded on FTO was measured with UV/Vis spectrophotometer (Solidspec-3700).

Electrochemical measurement

EC and PEC measurements were carried out in a three-electrode configuration. FTO was used as a working electrode for EC system, and CIGS was used for PEC measurements. Pt coil and Ag/AgCl (3 M KCl) were used as a counter and reference electrode, respectively. FTO surface and Mo back contact was connected to Sn–Cu wire with silver paste, and sealed with epoxy (Hysol 9460) leaving an active area of approximately 0.1 cm^2. The electrolyte consisted of a 0.5 M KPi buffer solution (0.5 M K_2SO_4, 0.5 M KH_2PO_4, 0.5 M K_2HPO_4) whose pH was adjusted to 6.8 by the addition of 1 M KOH. CV, LSV, and chronoamperometry were measured by a potentiostat (BiStat, Bio-Logic) with a scan rate of 20 mV s^{-1}. For PEC measurements, a 300 W Xe arc lamp (Oriel Instruments 66902) with an AM 1.5 G optical filter was used for 1 sun illumination, which was calibrated by a Si reference cell (PVM-580-BK7).

Acknowledgements

This research was supported by Nano·Material Technology Development Program(Green Nano Technology Development Program) through the National Research Foundation of Korea (NRF) funded by the Ministry of Education, Science and Technology (No. 2018 M3 A7B4065662), Nano·Material Technology Development Program through the National Research Foundation of Korea(NRF) funded by the Ministry of Science, ICT and Future Planning (2017 M3 A7B4049507), the National Research Foundation of Korea (NRF) grant funded by the Korea government (MSIT) (No. NRF-2018R1 A5 A1025594), and the Technology Development Program to Solve Climate Changes of the National Research Foundation (NRF) funded by the Ministry of Science, ICT & Future Planning (No. 2016 M1 A2 A2936757).

Conflict of Interest

The authors declare no conflict of interest.

Keywords: drop-casting · hydrogen reduction · nanocubes · photoelectrochemistry · water splitting

[1] D. Li, J. Shi, C. Li, *Small* **2018**, *14*, 1704179.
[2] X. Sun, X. Fu, T. You, Q. Zhang, L. Xu, X. Zhou, H. Yuan, K. Liu, *Electron. Mater. Lett.* **2018**, *14*, 733–738.
[3] W. H. Cheng, M. H. Richter, M. M. May, J. Ohlmann, D. Lackner, F. Dimroth, T. Hannappel, H. A. Atwater, H. J. Lewerenz, *ACS Energy Lett.* **2018**, *3*, 1795–1800.
[4] C. G. Morales-Guio, S. D. Tilley, H. Vrubel, M. Grätzel, X. Hu, *Nat. Commun.* **2014**, *5*, 3059.
[5] B. Koo, S. W. Nam, R. Haight, S. Kim, S. Oh, M. Cho, J. Oh, J. Y. Lee, B. T. Ahn, B. Shin, *ACS Appl. Mater. Interfaces* **2017**, *9*, 5279–5287.
[6] M. Tavakkoli, T. Kallio, O. Reynaud, A. G. Nasibulin, C. Johans, J. Sainio, H. Jiang, E. I. Kauppinen, K. Laasonen, *Angew. Chem. Int. Ed.* **2015**, *54*, 4535–4538; *Angew. Chem.* **2015**, *127*, 4618–4621.
[7] X. Zou, X. Huang, A. Goswami, R. Silva, B. R. Sathe, E. Mikmeková, T. Asefa, *Angew. Chem. Int. Ed.* **2014**, *53*, 4372–4376; *Angew. Chem.* **2014**, *126*, 4461–4465.

© 2021 Wiley-VCH GmbH

[8] J. Deng, P. Ren, D. Deng, L. Yu, F. Yang, X. Bao, *Energy Environ. Sci.* **2014**, *7*, 1919–1923.
[9] L. Wang, Y. Li, M. Xia, Z. Li, Z. Chen, Z. Ma, X. Qin, G. Shao, *J. Power Sources* **2017**, *347*, 220–228.
[10] J. Wang, S. Mao, Z. Liu, Z. Wei, H. Wang, Y. Chen, Y. Wang, *ACS Appl. Mater. Interfaces* **2017**, *9*, 7139–7147.
[11] Z. Zhang, P. Wang, *J. Mater. Chem.* **2012**, *22*, 2456–2464.
[12] J. Choi, J. T. Song, H. S. Jang, M. J. Choi, D. M. Sim, S. Yim, H. Lim, Y. S. Jung, J. Oh, *Electron. Mater. Lett.* **2017**, *13*, 57–65.
[13] Y. Li, H. Wang, L. Xie, Y. Liang, G. Hong, H. Dai, *J. Am. Chem. Soc.* **2011**, *133*, 7296–7299.
[14] F.-X. Ma, H. Bin Wu, B. Y. Xia, C.-Y. Xu, X. W. D. Lou, *Angew. Chem. Int. Ed.* **2015**, *54*, 15395–15399; *Angew. Chem.* **2015**, *127*, 15615–15619.
[15] W. F. Chen, K. Sasaki, C. Ma, A. I. Frenkel, N. Marinkovic, J. T. Muckerman, Y. Zhu, R. R. Adzic, *Angew. Chem. Int. Ed.* **2012**, *51*, 6131–6135; *Angew. Chem.* **2012**, *124*, 6235–6239.
[16] Q. Liu, J. Tian, W. Cui, P. Jiang, N. Cheng, A. M. Asiri, X. Sun, *Angew. Chem. Int. Ed.* **2014**, *53*, 6710–6714; *Angew. Chem.* **2014**, *126*, 6828–6832
[17] J. Duan, S. Chen, M. Jaroniec, S. Z. Qiao, *ACS Nano* **2015**, *9*, 931–940.
[18] Z. Bai, S. Li, J. Fu, Q. Zhang, F. Chang, L. Yang, J. Lu, Z. Chen, *Nano Energy* **2019**, *58*, 680–686.
[19] B. Cao, G. M. Veith, R. E. Diaz, J. Liu, E. A. Stach, R. R. Adzic, P. G. Khalifah, *Angew. Chem. Int. Ed.* **2013**, *52*, 10753–10757; *Angew. Chem.* **2013**, *125*, 10953–10957.
[20] H. Yin, S. Zhao, K. Zhao, A. Muqsit, H. Tang, L. Chang, H. Zhao, Y. Gao, Z. Tang, *Nat. Commun.* **2015**, *6*, 6430.
[21] Y. Chen, K. Sun, H. Audesirk, C. Xiang, N. S. Lewis, *Energy Environ. Sci.* **2015**, *8*, 1736–1747.
[22] J. Kye, M. Shin, B. Lim, J. W. Jang, I. Oh, S. Hwang, *ACS Nano* **2013**, *7*, 6017–6023.
[23] N. Cheng, S. Stambula, D. Wang, M. N. Banis, J. Liu, A. Riese, B. Xiao, R. Li, T. K. Sham, L. M. Liu, G. A. Botton, X. Sun, *Nat. Commun.* **2016**, *7*, 13638.
[24] K. Jiang, B. Liu, M. Luo, S. Ning, M. Peng, Y. Zhao, Y. R. Lu, T. S. Chan, F. M. F. de Groot, Y. Tan, *Nat. Commun.* **2019**, *10*, 1743.
[25] S. Ye, F. Luo, Q. Zhang, P. Zhang, T. Xu, Q. Wang, D. He, L. Guo, Y. Zhang, C. He, X. Ouyang, M. Gu, J. Liu, X. Sun, *Energy Environ. Sci.* **2019**, *12*, 1000–1007.
[26] X. Cheng, Y. Li, L. Zheng, Y. Yan, Y. Zhang, G. Chen, S. Sun, J. Zhang, *Energy Environ. Sci.* **2017**, *10*, 2450–2458.
[27] J. Seo, S. Lee, B. Koo, W. Jung, *CrystEngComm* **2018**, *20*, 2010–2015.
[28] S. Lee, J. Seo, W. Jung, *Nanoscale* **2016**, *8*, 10219–10228.
[29] P. Strasser, M. Gliech, S. Kuehl, T. Moeller, *Chem. Soc. Rev.* **2018**, *47*, 715–735.
[30] W. Sheng, Z. Zhuang, M. Gao, J. Zheng, J. G. Chen, Y. Yan, *Nat. Commun.* **2015**, *6*, 5848.
[31] Y. Borodko, L. Jones, H. Lee, H. Frei, G. Somorjai, *Langmuir* **2009**, *25*, 6665–6671.
[32] B. Koo, D. Kim, P. Boonmongkolras, S. R. Pae, S. Byun, J. Kim, J. H. Lee, D. H. Kim, S. Kim, B. T. Ahn, S. W. Nam, B. Shin, *ACS Appl. Mater. Interfaces* **2020**, *3*, 2296–2303.
[33] B. Koo, S. Byun, S. W. Nam, S. Y. Moon, S. Kim, J. Y. Park, B. T. Ahn, B. Shin, *Adv. Funct. Mater.* **2018**, *28*, 1705136.

Manuscript received: March 24, 2021
Accepted manuscript online: April 28, 2021
Version of record online: May 18, 2021

© 2021 Wiley-VCH GmbH